Acceleration and orbits of charged particles beneath a monolayer plasma crystal

V. A. Schweigert and I. V. Schweigert[a]
Institute of Theoretical and Applied Mechanics, 630090 Novosibirsk, Russia

V. Nosenko and J. Goree[b]
Department of Physics and Astronomy, The University of Iowa, Iowa City, Iowa 52242

Experiments and simulations are reported for a monolayer plasma crystal that is disturbed by an extra particle moving in a plane below the monolayer. Numerical simulations and experiments are performed to find an explanation for the motion of the extra particle. In contrast to earlier simulations where an extra particle did not move spontaneously as in the experiment, here an ion wakefield downstream of the monolayer of particles is included. This resulted in the spontaneous motion of an extra particle as in the experiment, so that it is concluded that the wakefield produces this motion. In both the experiment and the simulation a trend is observed where the orbit of an extra particle becomes more crooked and less energetic when the gas damping is stronger. The simulation reveals that the energy of the extra particle exhibits distinctive transitions between three regimes. © *2002 American Institute of Physics.* [DOI: 10.1063/1.1512656]

I. INTRODUCTION

Plasma crystals are ordered structures of charged microspheres in a gas discharge.[1-6] The low-temperature plasma charges the microsphere particles negatively up to 10^4 elementary charges, so that the particle ensemble is a strongly coupled classical Coulomb system. In the sheath of a rf discharge, particles are trapped in a horizontal layer. In the vertical direction, they are confined by the opposing forces of gravity and an upward electrical force in the electric sheath near a horizontal electrode. In the radial direction, they are confined by the plasma's radial electric fields, which are much weaker and allow particle movement in the horizontal direction. Depending on the electrode configuration and the number of particles that are introduced into the plasma, the particles can arrange in a monolayer[7] or in a three-dimensional structure with multiple layers.[6,8] The particles arrange themselves in lattices with a crystalline pattern, making them useful as models for studying condensed matter phenomena.

In this paper we will investigate the dynamics of a particle structure with a crystalline monolayer on a horizontal plane, and beneath it an extra particle moving about in what we term an "incomplete lower layer." The monolayer is a triangular lattice with hexagonal symmetry.

In the experiments of Samsonov *et al.*,[7,9] a kind of spontaneous particle motion was observed. The experiments were performed using a monolayer of particles, with a few extra particles in an incomplete second layer 200 μm below the monolayer. These extra particles moved about spontaneously, and through a Coulomb interaction, they disturbed the particles in the main layer. Samsonov *et al.* discovered that this motion resulted in the generation of a Mach cone, i.e., a

V-shaped wake made of compressional sound waves, in the monolayer.

The mechanism that accelerates the particles must be a persistent force, because it overcomes the constant friction experienced by the extra particle as it moves in the gas.[10] Presumably the accelerating mechanism is an electric force, but the mechanism behind it until now has not been identified.

The simulation of Schweigert *et al.*[11] included extra particles similar to those in Samsonov's experiment, except that the simulations included an additional complete monolayer, for a total of two complete monolayers plus an incomplete third layer beneath. The simulation revealed that the particle motion had two distinct regimes, depending on the damping rate, before the crystal melted entirely by further reduction of the gas pressure. The orbits of extra particles in the incomplete third layer shown in Fig. 9 of Ref. 11 are more crooked than in the experiment of Samsonov.

Here we report further simulations, which have only a single monolayer and an incomplete lower layer, as in the experiment of Samsonov. This configuration does not melt as easily as with two complete monolayers; therefore, we were able to extend the simulation to lower values of the gas pressure, and observe straighter orbits like those of Samsonov *et al.* In the present paper we also report experiments, and comparing them to the simulations allows us to draw a conclusion about the acceleration mechanism.

We first carried out simulations, using the parameters of the experiment of Samsonov *et al.*,[7] who did not report any images of the extra particle's orbit. We repeated the simulations for several values of the damping rate corresponding to several values of the gas pressure. After the simulations were completed, we carried out the new experiments, intended to record the orbits of the fast particles over roughly the same conditions as in the simulation.

[a]Electronic mail: ischweig@itam.nsc.ru
[b]Electronic mail:

II. SIMULATION

We used molecular dynamics (MD) simulations to observe the motions of all particles in a monolayer, plus an extra particle beneath it. We modeled a section of a suspension that included $N=1024$ particles, and we applied periodic boundary conditions. To start the MD simulation, particles were loaded initially with a Maxwellian velocity distribution. Their motion was constrained to move in the horizontal plane $z=0$ and they arranged themselves in a triangular lattice with hexagonal symmetry, as in the experiments. The extra particle was constrained to move on another horizontal plane at $z=-200$ μm below the monolayer. The equations that were solved for particles in the monolayer crystal, with coordinates $\boldsymbol{\rho}_i$, where i ranges from 1 to N, were

$$M_p \frac{d^2 \boldsymbol{\rho}_i}{dt^2} = -Z \frac{\partial U_u(\boldsymbol{\rho}_i - \boldsymbol{\rho}_e)}{\partial \boldsymbol{\rho}_i} - Z \sum_{i \neq j} \frac{\partial U_i(\boldsymbol{\rho}_i - \boldsymbol{\rho}_j)}{\partial \boldsymbol{\rho}_i}$$

$$- M_p \nu \frac{d\boldsymbol{\rho}_i}{dt} - \mathbf{F}_L. \quad (1)$$

For the extra particle with coordinates $\boldsymbol{\rho}_e$ we solved

$$M_p \frac{d^2 \boldsymbol{\rho}_e}{dt^2} = -Z \sum_i \frac{\partial U_l(\boldsymbol{\rho}_e - \boldsymbol{\rho}_i)}{\partial \boldsymbol{\rho}_e} - M_p \nu \frac{d\boldsymbol{\rho}_e}{dt} - \mathbf{F}_L. \quad (2)$$

Here $\mathbf{F}_L$ is the random Langevin force acting on the particles due to collisions with neutral gas atoms with a gas temperature T. The first and the second terms on the right-hand side of Eq. (1) are the forces acting on the ith particle from the extra particle beneath and from other particles of the monolayer (and from their periodic images), respectively. On the right-hand side of Eq. (2) the first term is the force applied by the monolayer particles to the extra particle. The friction coefficient ν arises from the drag on the particle due to the neutral gas, and it is modeled as Epstein drag.[10] The particle mass in the MD simulations was $M_p = 3.7 \times 10^{-10}$ g.

The primary difference between our MD simulation and the simulation in Ref. 7 is the interparticle potential. The simulation of Ref. 7 used a simple Yukawa interparticle potential, which was adequate for producing a Mach cone in the monolayer but cannot result in a spontaneous motion of an extra particle. It was necessary in that simulation to artificially move the extra particle. Here, we will use a different interparticle interaction, described in the following, and will demonstrate that it results in a spontaneous motion, as in the experiment.

The interparticle interaction was determined accurately by performing a particle-in-cell Monte Carlo (PIC MC) simulation including the particles in the monolayer, electrons, and ions, as described earlier in Ref. 12. For these *ab initio* simulations we chose the conditions of the experiment of Samsonov *et al.*[7] The input rf power was 50 W, and the ion density n_i in the sheath was 9.75×10^9 cm^{-3}. We assumed krypton at gas pressure $P=5$ Pa and temperature $T=300$ K. In both the PIC MC and MD simulations, all particles have the same diameter of 8.9 μm and charge $Z=-15\,000$ e. The horizontal interparticle spacing of $a=256$ μm was the same as in the experiment of Samsonov
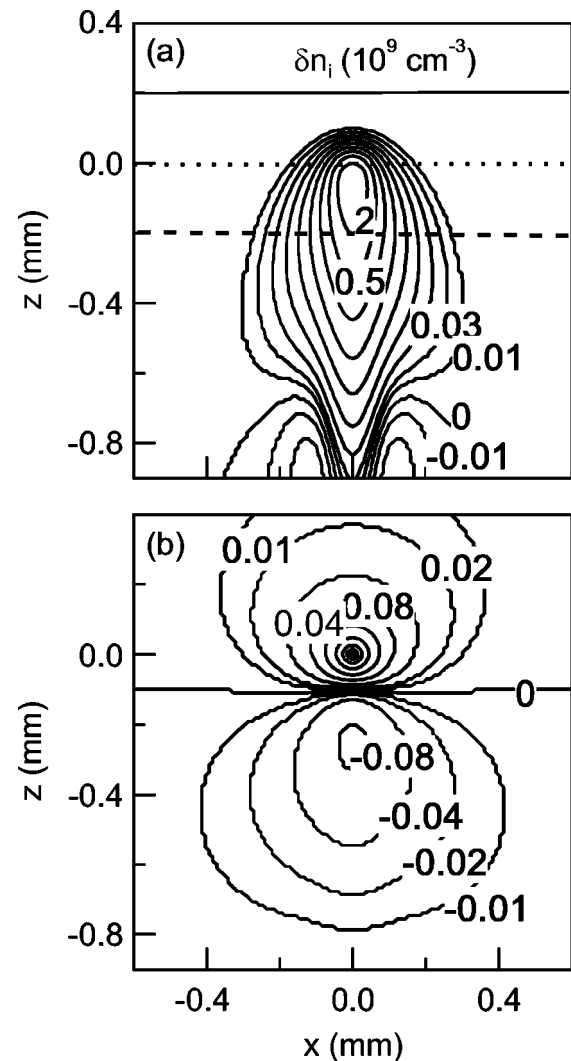
FIG. 1. Perturbation of ion density (a) and perturbation of electrical potential measured in electron volts (b) surrounding a single particle placed at ($x=0$, $z=0$) at the height of the monolayer in the sheath. These data are from a PIC MC simulation. Ions flow into the simulation box in the $-z$ direction. Ion density perturbation δn_i is in units of 10^9 cm^{-3}. The dotted line denotes the position of the monolayer, and the dashed line refers to the horizontal plane in which the extra particle moves.

et al. The ion density perturbation and the potential distribution around the particle in the monolayer obtained in PIC MC simulation is shown in Fig. 1. One can see that the ion density perturbation between the monolayer and the extra particle is more than 2×10^9 cm^{-3}. For these experimental conditions the ion flux is supersonic and the ion cloud is elongated. The dimensionless ratio of the drift and thermal ion velocities is $M=11.9$.

To calculate the forces acting on the particles in Eqs. (1) and (2), we model the potential computed from the *ab initio* PIC MC calculations using the following analytic expressions. In the following expressions, the potentials have units of ergs and the interparticle distance is measured in centimeters. The particle potential U_i in the crystal lattice is assumed to be a Debye–Huckel type,

$$U_i(\boldsymbol{\rho}_i - \boldsymbol{\rho}_j) = \frac{Ze^2}{|\boldsymbol{\rho}_i - \boldsymbol{\rho}_j|} \exp(-\kappa_i |\boldsymbol{\rho}_i - \boldsymbol{\rho}_j|/a),$$
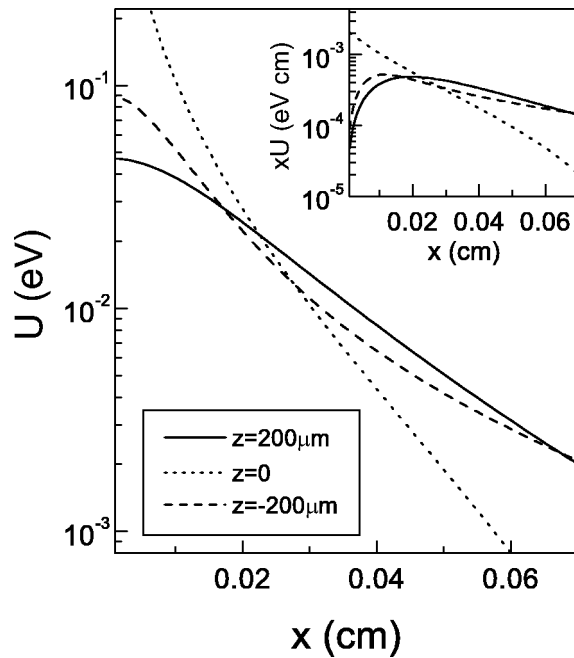
FIG. 2. Potential distributions around a particle from the PIC MC simulation as a function of the x coordinate, i.e., the coordinate perpendicular to the ion flow. Three curves correspond to the three horizontal lines in Fig. 1, for $z=0.02$, 0, and -0.02 cm. The inset shows $xU(x)$ as a function of the horizontal distance x.

where the effective screening length $\kappa_i=1.64$ and $|\boldsymbol{\rho}_i-\boldsymbol{\rho}_j|$ is the interparticle distance between the particles belonging to the monolayer. The extra particle acts on a particle above it, in the monolayer, with a force determined by the following interparticle potential:

$$U_u(\boldsymbol{\rho}_i-\boldsymbol{\rho}_e)=\frac{Z_1e^2}{|\boldsymbol{\rho}_i-\boldsymbol{\rho}_e|}\exp(-\kappa_e|\boldsymbol{\rho}_i-\boldsymbol{\rho}_e|/a),$$

where $Z_1=12\,930$, $\kappa_e=0.916$, and $|\boldsymbol{\rho}_i-\boldsymbol{\rho}_e|$ is the distance between a particle in the monolayer and the extra particle. For computing the force acting on the extra particle from a particle in the monolayer we use the potential

$$U_l(\boldsymbol{\rho}_e-\boldsymbol{\rho}_i)=\frac{Z_2e^2}{a}\exp(-\kappa_l|\boldsymbol{\rho}_e-\boldsymbol{\rho}_i|/a)(-a/|\boldsymbol{\rho}_e-\boldsymbol{\rho}_i|$$
$$+0.156(a/|\boldsymbol{\rho}_e-\boldsymbol{\rho}_i|)^3-1.1(a/|\boldsymbol{\rho}_e-\boldsymbol{\rho}_i|)^5),$$

where $Z_2=4905$, $\kappa_l=0.559$, and $|\boldsymbol{\rho}_e-\boldsymbol{\rho}_i|$ is the distance between the extra particle and a particle in the monolayer. For illustration we show in Fig. 2 the absolute values of the particle potential in different horizontal planes: U_i (dotted line) and U_u (solid line) are repulsive positive potentials, while U_l (dashed line) is an attractive potential which has a negative value. The inset in Fig. 2 shows $xU(x)$, revealing a discrepancy as compared to the Yukawa potential.

Note that the interparticle potential is not symmetric, between the particle in the monolayer and a particle in the incomplete lower layer. The attractive potential U_l is larger than the repulsive U_u by about a factor of 2 when the extra particle sits in the vertically aligned position. In other words, $U_u \neq U_l$. This situation arises because the system is not closed. Ions are generated upstream of the particles and they flow past the microspheres. This phenomenon was reported previously[13,14] for the analysis of instabilities in bilayer crystals. In a bilayer crystal this asymmetry causes an instability to develop, thereby introducing enough energy to melt the lattice, unless the gas pressure is sufficiently high to suppress the instability. Our present problem is different because in our lower layer there is only a single extra particle. Otherwise the same interparticle mechanisms apply as in the case of the bilayer crystal.

The PIC MC simulations are the most time-consuming part of our calculations. For this reason, in the MD simulation we use the interparticle potential calculated for a gas pressure of 5 Pa in all our cases, even for pressures different from 5 Pa. Elsewhere in the MD simulation, the gas pressure also appears in the friction coefficient. We calculate the friction coefficient ν for each gas pressure using the Epstein formula.[10]

In the simulations, we intended to duplicate the conditions of the experiment of Samsonov et al.[7] Our experiments, reported in this paper, were carried out after the simulations were completed. As mentioned previously, the interparticle potential that we used was calculated for only one of the gas pressures, and this was applied to all the MD simulations, for all gas pressures. These various differences, as compared to our experiment, are generally in the range of 50% to a factor of 3; therefore, we do not expect to achieve exact quantitative agreement between the simulation and experiment. The general features of the particle orbit shape and its trends, as the gas pressure is varied, show agreement, as we will demonstrate in Sec. IV. This agreement is perhaps the most that one can expect, given the quantitative differences in the parameters of the simulation and experiment.

The goals of our simulation are to: (1) identify the acceleration mechanism for the extra particles and (2) present phenomenological results for the shape of the extra particle's orbit and its energy in different regimes of motion. In our MD simulation, we also observed Mach cones in the monolayer, produced by the moving extra particle. This observation of Mach cones is similar to the experimental observation of Samsonov et al.[7] Because the Mach cones were previously revealed in the simulation of Ref. 7, and our results are similar, we do not report them further here. Instead, we will pursue the three goals listed previously, and compare to the new experimental results also reported in the present paper.

III. EXPERIMENT

The experimental part of this work was carried out using the same apparatus as used in Ref. 7. We used a capacitively coupled rf discharge to produce a krypton plasma. The discharge apparatus is shown in Fig. 3. A lower electrode was powered with a rf high voltage at 13.56 MHz. A grounded upper ring and the vacuum vessel walls served as the other electrode. The gas flow rate of 0.45 sccm was small enough to avoid disturbing the particles. After igniting a plasma, we
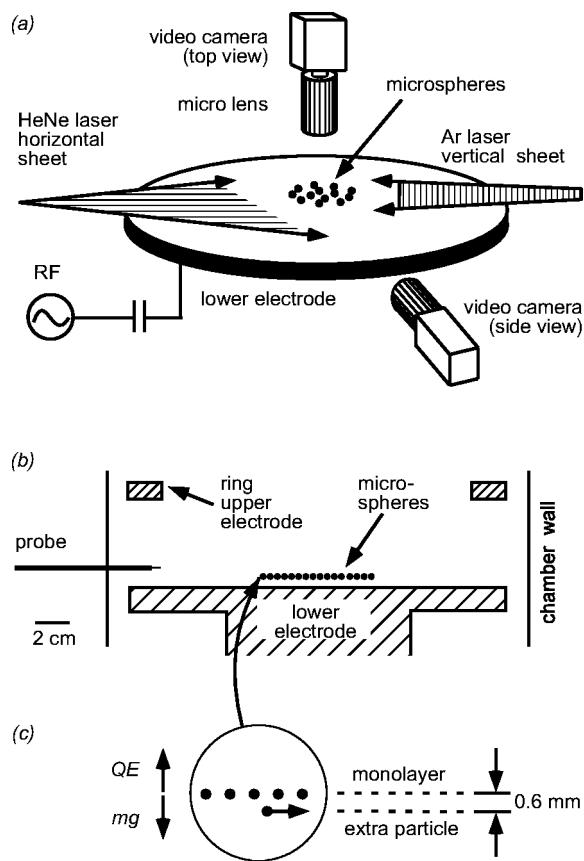
FIG. 3. Experimental apparatus: (a) general view, (b) schematic side view, and (c) locations of the two-dimensional monolayer and an extra particle, which moves horizontally in an incomplete second layer ≈0.6 mm below the monolayer.

introduced monodisperse polymer microspheres with a diameter of 8.09 ± 0.18 μm measured using transmission electron microscopy (TEM). They were shaken from a dispenser that we inserted above the lower electrode inside the vacuum vessel. To image the particles, we illuminated them with a HeNe laser beam expanded by a rotating mirror into a hori-

zontal sheet, and we imaged them with a vertically mounted monochrome video camera operated at 30 frames/s. The camera was equipped with an interference bandpass filter to image only the scattered laser light.

In the experiment, particles were levitated in a single horizontal layer, and they arranged in a triangular lattice with hexagonal symmetry. In contrast to a multilayer system, a monolayer crystal is much less sensitive to variation of experimental conditions such as gas pressure and rf voltage. Over a wide range of discharge parameters, the experimental monolayer remained in a crystalline state with a translational order length of $(1.6-2.6)a$ and an orientational order length of $(2.4-6.0)a$, as shown in Table I. These rather low values suggest, however, that the monolayer, while crystalline, was not highly ordered.

When a sufficient number of particles were introduced, we always found extra particles levitated in an incomplete lower layer. These particles moved about, disturbing the layer above. In the case of the highest gas pressure we used, and possibly in other cases as well, the extra particles appeared to be brighter than particles in the monolayer. This indicates that the extra particles were probably bigger, being possibly agglomerations of two or three microspheres.

In the experiment we varied the gas pressure from $P = 2.7$ to 11.7 Pa, thereby varying the damping rate. We adjusted the gas pressure until we observed orbits that resembled those in the simulation, for all three regimes. The main experimental parameters are listed in Table I. Experimental values for charge were measured using a variant of the resonance method of Ref. 15, which is accurate within a factor of 2.

IV. RESULTS

A. Acceleration mechanism

One of our main results is a conclusion that the mechanism of accelerating the extra particle must arise from the ion wakefield. Here we will review the results, and then present an argument that supports our conclusion.

TABLE I. Discharge conditions and lattice parameters for the experiment.

Discharge conditions			
Pressure of Kr (Pa)	2.7	9.2	11.7
Power (W)	110	70	100
Self-bias voltage (V)	−177	−122	−137
Electron temperature (eV)	3.5	1.7	2.6
Ion density (10^{15} m^{-3})	2.7	10.1	13.1
Debye length at probe height, λ_D (μm)	267	97	106
Epstein drag, ν (s^{-1})	5.7	19.3	24.5
Structural parameters for the lattice			
Particle separation, a (μm)	529 ± 2	495 ± 1	601 ± 1
Translational order length, ξ/a	2.6 ± 0.2	1.9 ± 0.1	1.6 ± 0.1
Orientational order length, ξ_6/a	6.0	2.6	2.4
Monolayer height (mm)	9.0	6.1	5.2
Extra particle height (mm)	8.4	5.5	4.5
Experimental parameters for the lattice			
Particle charge, Q	16 600	11 700	8300
Dust plasma frequency, ω_{pd} (s^{-1})	113.1	88.0	46.7
ν/ω_{pd}	0.05	0.22	0.52

In Fig. 4, simulation and experimental results both show an acceleration of the extra particle. In our MD simulation the extra particle initially has a kinetic energy equivalent to room temperature, and then it gradually gains energy with time. The acceleration of the particle ceases when it reaches a terminal velocity of, for example, 4.2 cm/s at a pressure $P=5$ Pa. Without any acceleration mechanism, the extra particle would not move any more than other particles, because gas damping removes any excess energy in the particle motion. The fact that the extra particle moves faster than the other particles shows that it receives a constant energy input; i.e., it is accelerated. We also note, in Fig. 4, that the particle motion depends on the gas pressure and therefore the damping rate. Comparing Figs. 4(a)–4(f), we find the same trend in both the experiment and the simulation: as the damping rate is decreased, the extra particle moves a greater distance.

The fact that our experiment and simulation agree in the acceleration of the extra particle suggests that the simulation incorporates the physics responsible for the acceleration. As compared to the MD simulation of Ref. 7, where the particle did not accelerate spontaneously, the primary difference is that the interparticle potential in our simulation takes into account the ion wakefield. Thus, we attribute the acceleration of the particles to the wakefield.

The extra particle is accelerated due to the instability of the configuration consisting of a monolayer of particles plus an extra particle. This instability arises due to the asymmetric interaction between a particle in the monolayer and the extra particle, caused by the effect of ion wakefield, as explained in Sec. II. At a higher gas pressure, this instability is suppressed by the gas friction. A decrease of the gas friction below some critical value initiates development of the instability. The source of energy to this system is provided by the flux of streaming ions, so that this system is open rather than closed.

B. Effect of gas damping on the extra particle's orbit

As another of our main results, we find that in both the experiment and the MD simulations the extra particle's trajectory depends on the gas pressure. More precisely, it depends on the dimensionless friction coefficient ν/ω_{pd}, which is the ratio of the friction coefficient and the dust crystal frequency $\omega_{pd}=\sqrt{Z^2e^2/\epsilon_0 M_p a^3}$. This dimensionless friction coefficient was introduced in Refs. 13 and 14 for characterizing the instability in the bilayer vertically aligned crystal. The range of the dimensionless friction coefficient ν/ω_{pd} in the experiment and in MD simulation coincides. At a higher level of gas damping (for 11.7 Pa in the experiment), the extra particle is trapped beneath a single particle in the monolayer, as shown in Figs. 4(a) and 4(b). The left panel (a) is from the simulation, and the right (b) is from the experiment. At a lower level of gas damping, the extra particle has a stretched trajectory. The extra particle is scattered less often than at higher gas damping, where it has a more crooked orbit. This is seen by comparing Figs. 4(c) and 4(d), at a higher gas damping, to Figs. 4(e) and 4(f) at a lower gas damping. At a low level of gas damping, the extra particle moves mainly in a straight line over a distance of many

interparticle spacings, as shown by the trajectories in Figs. 4(e) and 4(f). This is one of our chief empirical results: the orbit of the extra particle has the same shape, in the simulation and the experiment, and the shape has the same trend of becoming straighter as the gas damping is reduced.

While the shape of the extra particle orbits are the same in the experiment and the simulation, the speed of the extra particle does not always agree. For our lowest gas damping rate, the simulated and experimental orbits shown in Figs. 4(e) and 4(f) have almost the same speeds for the extra particle. However, for the intermediate damping rate, the speeds in Figs. 4(c) and 4(d) differ by a factor of 3.3. Exact agreement is not expected because in the experiment the speed of the extra particle varies over a factor of 2, from one particle to another.[9] Another reason for the discrepancies observed might be the difference between the experimental parameters and those used in the simulations.

The conditions in the experiment and the simulations were similar but not identical. The interparticle spacing and the vertical spacing between the extra particle and the monolayer are not exactly the same. In the simulation, the particles have a nearly uniform interparticle spacing that extends infinitely in all directions, because of the periodic boundary conditions. In the experiment, a finite number of particles are confined in a bowl-shaped electric potential well, and this causes the particles to be spaced more closely in the center of the suspension than at the edges. This arrangement leads to a larger number of defects in the experiment than in the simulation. Thus, the particles in the monolayer present a more highly periodic potential structure in the simulation than in the experiment; in both cases the particles form a crystal, but the crystal is more ordered in the simulation than in the experiment.

In the experiment we chose only three gas pressures, as compared to a larger number of values in the simulations. We adjusted the gas pressure in the experiment until we observed particle orbits that resembled those in each of the three regimes of particle motion in the simulations.

V. TRANSITIONS BETWEEN THREE REGIMES OF MOTION

Our primary purposes in this paper are to report phenomenological observations from the experiment and simulations, and compare those to arrive at an explanation for the acceleration mechanism. Beyond those results, which were presented in Sec. IV, we will now report some phenomenological results from the simulation revealing distinctive transitions between three regimes of particle motion. The shapes of the particle trajectories are different in each regime. While we do not attempt to explain intuitively the exact shapes of the particle orbits, we can offer some comments on mechanisms that are involved.

In the simulation, we found that as we varied the gas damping, the motion of the extra particle had three distinct regimes, with transitions between them. Within each regime, the particle motion was generally about the same. However, near a critical value of gas damping, a small change in gas pressure resulted in a significantly different kind of motion
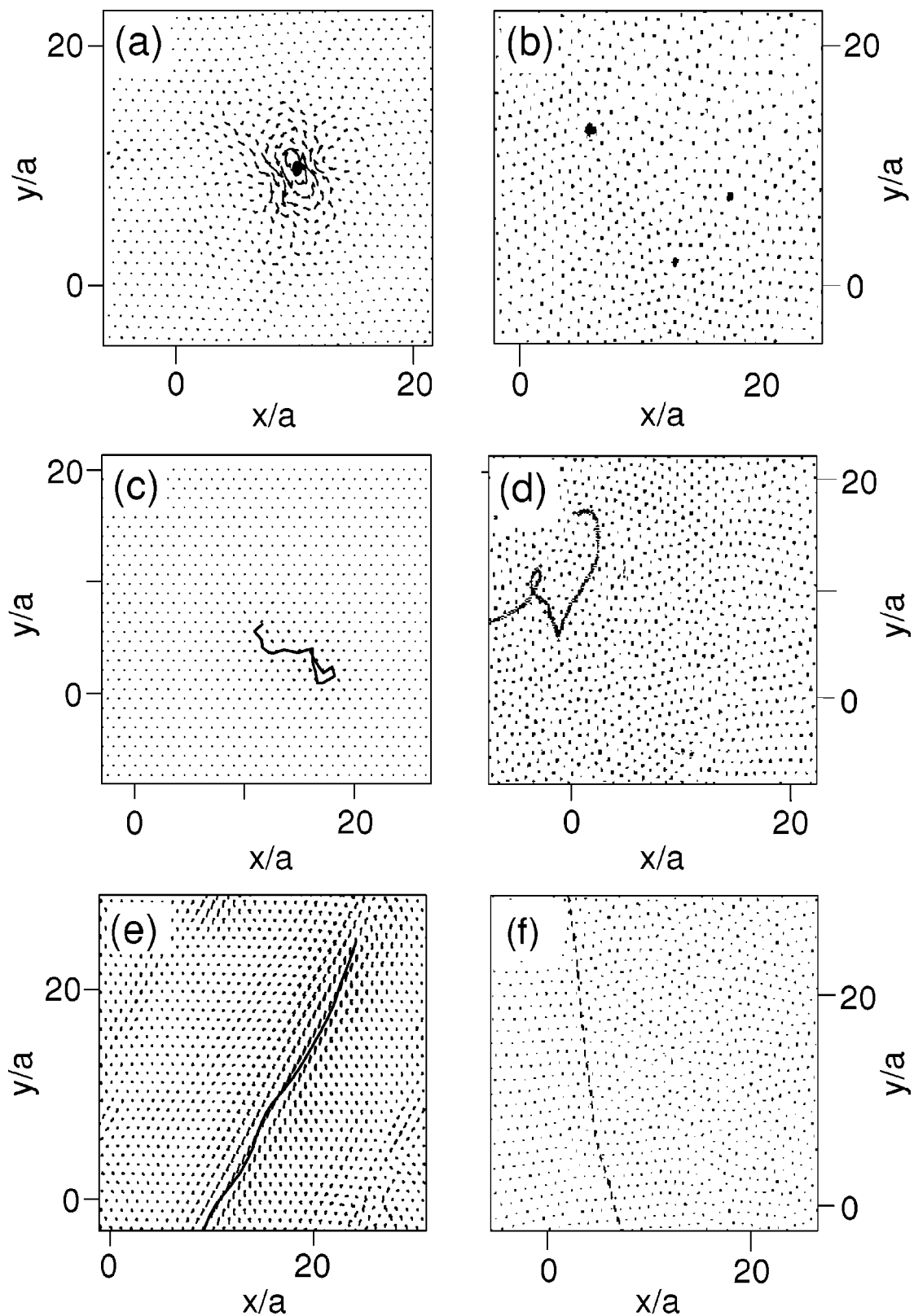
FIG. 4. Trajectories of particles in the monolayer and the extra particle beneath (thicker line) in the simulation (left-hand column), and in the experiment (right-hand column). The conditions in the simulations and experiment were similar but not identical. In the high pressure range, the damping rates were (a) $\nu=0.3\ \omega_{pd}$ in the simulations and (b) 0.52 ω_{pd} in the experiment. In the middle regime, it was (c) 0.14 ω_{pd} and (d) 0.22 ω_{pd}, respectively. In the low pressure regime, (e) 0.03 ω_{pd} and (f) 0.05 ω_{pd}. The length is normalized by the interparticle distance a. The time interval for the orbits shown are (a),(c),(e) 0.2 s, (b),(d) 2 s, and (f) 0.6 s. The orbits of particles in the experiment and simulation can be compared for the extra particles, but not for particles in the monolayer, for which we present only a single-frame snapshot from the experiment rather than a trace of multiple trajectories as in the simulation.

Phys. Plasmas, Vol. 9, No. 11, November 2002

Acceleration and orbits of charged particles . . .   4471
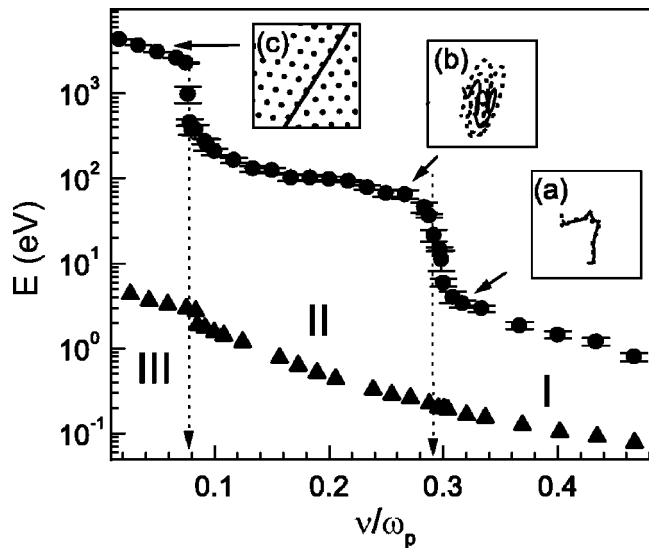
FIG. 5. Regimes of motion of the extra particle: (I) "molecular" state, (II) diffusion, (III) straight-line motion. The mean kinetic energy of particles in the monolayer (triangles) and the extra particle (circles) are plotted as a function of the dimensionless friction coefficient. The energy of the extra particle undergoes two transitions, where a small change in friction results in a large change in particle energy. The insets show the enlarged trajectories of the particles (a) at $\nu = 0.3\ \omega_{pd}$, (b) at $\nu = 0.27\ \omega_{pd}$, and (c) at $\nu = 0.03\ \omega_{pd}$. The size of the inset boxes is 0.1×0.1 mm^2 for (a) and (b), and 2×2 mm^2 for (c). The trajectory of the extra particle in the incomplete lower layer is shown by a solid line, and that of the upper layer by a dashed line in (a) and (b). In (c) the particles in the upper layer are shown in a snapshot.

of the extra particle. This is shown in Fig. 5. At a higher pressure (regime I), an extra particle and a particle in the monolayer remain aligned, in a sort of vertically aligned "molecule." In Fig. 5, for $\nu = 0.3\ \omega_{pd}$, inset (a) shows the trajectories of two particles composing a vertical "molecule" for a 0.2 s interval. The ion cloud beneath the upper particle moves with the upper particle, and it does so without any significant lag because the ions can move much more quickly than the particle. For this reason, the lower particle can couple easily to the upper particle not only when the latter is at rest, but also when it is moving. This coupling persists when the attraction energy between particles is less than the kinetic energy of the extra particle. The monolayer of charged particles produces a periodic potential distribution below which the extra particle moves in. At $\nu = 0.3\ \omega_{pd}$ the kinetic energy of the particle is much less than the depth of the potential wells, and the extra particle is trapped.

The first transition occurs with a small decrease of the friction coefficient from $\nu = 0.3\ \omega_{pd}$ to $\nu = 0.27\ \omega_{pd}$. This results in a large increase in the kinetic energy of the extra particle from 5 to 80 eV, causing the "molecule" to dissociate. The motion in regime II of Fig. 5 is diffusive. Inset (b) to Fig. 5 shows the trajectories of the monolayer particle and the extra particle in regime II very near to transition at $\nu = 0.27\ \omega_{pd}$. Decreasing the pressure further, the energy of particle rises and, consequently, the probability of jumps between the equilibrium places increases, as shown in Figs. 4(c) and 4(d).

This first transition between regimes I and II was reported earlier in Ref. 11 for a slightly different system, with two complete layers and a few extra particles beneath the lower layer. The curve in Fig. 5 for our present results, for a single monolayer and an extra particle beneath, differs in the shape of the transition curve. Our curve has a sharper transition, and it occurs at a higher damping rate of $\nu/\omega_{pd} = 0.27$–0.3, as compared to ≈ 0.21.

The second transition occurs also with a small change of the friction coefficient, this time at $\nu = 0.08\ \omega_{pd}$. This results in another large increase in the energy of the extra particle, up to 1000 eV. This kinetic energy is higher than the attraction energy, so that the extra particle is not tightly coupled to a single particle above it. Now the particle trajectory is undisturbed straight line (regime III in Fig. 5) as shown in inset (c). This second transition was not previously reported in Ref. 11, where the pressure range did not extend to these low values.

The reason that the kinetic energy of a particle in a bilayer suspension changes quickly at some critical gas pressure was explained in Ref. 13. There it was shown that a multilayer structure with vertical alignment is unstable, causing a heating of the particles. At a higher pressure, gas friction suppresses the particle oscillations, and the extra particle is trapped by a potential well created by a particle in the upper layer. At a lower gas pressure, the extra particle's kinetic energy is comparable to the potential well's depth, and the extra particle can jump between wells and exhibit a diffusion-like motion. Thus, at this critical value for the friction, a decrease of gas pressure causes a distinctive transition between regimes of motion of the extra particle. At an even lower gas pressure, the kinetic energy of the extra particle exceeds the depth of the potential well so that the extra particle moves without deflection by individual particles in the monolayer. Moreover, in Ref. 14 the melting transition in the bilayer crystal was described as occurring in two steps. In the present paper, for a monolayer with an extra particle beneath, we observe a similar two-step transition in particle heating. Although our monolayer did not melt, we attribute our transition to the asymmetric particle interaction.

These transitions between distinct regimes reported here were found only in the simulation. To detect these in the experiment would require far more data, for many values of the gas pressure, than we recorded.

VI. CONCLUSIONS

We have found that the mechanism that accelerates an extra particle in an incomplete second layer of a plasma crystal is the asymmetric interparticle interaction between particles in the upper and lower layers. This asymmetry arises from the ion wakefield surrounding a particle in the presence of flowing ions. This finding is supported by general agreement between experiment and a MD simulation that includes an appropriate asymmetric interparticle potential. The agreement we find in our phenomenological results includes a similar shape in the particle orbits, and a tendency for the orbits to be long and straight in the absence of significant gas damping, and more crooked as the gas damping is increased. This agreement with a relatively clean and simple experiment also serves to validate the simulation model.

In the simulation we found that particle orbits in the incomplete lower layer have several distinct regimes. When the gas damping is changed by a small amount, transition takes place, with a significant jump in the kinetic energy of an extra particle.

ACKNOWLEDGMENTS

[1] J. H. Chu and L. I, Phys. Rev. Lett. **72**, 4009 (1994).
[2] H. Thomas, G. E. Morfill, V. Demmel, J. Goree, B. Feuerbacher, and D. Möhlmann, Phys. Rev. Lett. **73**, 652 (1994).
[3] Y. Hayashi and K. Tachibana, Jpn. J. Appl. Phys., Part 2 **33**, L804 (1994).
[4] A. Melzer, T. Trottenberg, and A. Piel, Phys. Lett. A **191**, 301 (1994).
[5] Y. Hayashi, Phys. Rev. Lett. **83**, 4764 (1999).
[6] J. B. Pieper, J. Goree, and R. A. Quinn, Phys. Rev. E **54**, 5636 (1996).
[7] D. Samsonov, J. Goree, Z. W. Ma, A. Bhattacharjee, H. M. Thomas, and G. E. Morfill, Phys. Rev. Lett. **83**, 3649 (1999).
[8] M. Zuzic, A. V. Ivlev, J. Goree, G. E. Morfill, H. M. Thomas, H. Rothermel, U. Konopka, R. Stterlin, and D. D. Goldbeck, Phys. Rev. Lett. **85**, 4064 (2000).
[9] D. Samsonov, J. Goree, H. M. Thomas, and G. E. Morfill, Phys. Rev. E **61**, 5557 (2000).
[10] P. Epstein, Phys. Rev. **23**, 710 (1924).
[11] I. V. Schweigert, V. A. Schweigert, A. Melzer, and A. Piel, Phys. Rev. E **62**, 1238 (2000).
[12] V. A. Schweigert, V. M. Bedanov, I. V. Schweigert, A. Melzer, and A. Piel, JETP **88**, 482 (1999).
[13] V. A. Schweigert, I. V. Schweigert, A. Melzer, A. Homann, and A. Piel, Phys. Rev. E **54**, 4155 (1996).
[14] V. A. Schweigert, I. V. Schweigert, A. Melzer, A. Homann, and A. Piel, Phys. Rev. Lett. **80**, 5345 (1998).
[15] Th. Trottenberg, A. Melzer, and A. Piel, Plasma Sources Sci. Technol. **4**, 450 (1995).